Poly(butylene terephthalate)/Clay Nanocomposite Compatibilized with Poly(ethylene-*co*-glycidyl methacrylate). I. Isothermal Crystallization

Jiann-Wen Huang

Department of Styling and Cosmetology, Tainan University of Technology, Yung Kang City, 710 Taiwan, Republic of China

Received 1 February 2008; accepted 28 May 2008
DOI 10.1002/app.28819
Published online 11 August 2008 in Wiley InterScience (www.interscience.wiley.com).

ABSTRACT: Poly(butylene terephthalate) (PBT)/clay nanocomposite was prepared by blending PBT and commercial modified montmorillonite clays via a extruder by using poly(ethylene-*co*-glycidyl methacrylate) (PEGMA) as a compatibilizer (PBT/PEGMA/Clay). PEGMA and clay were also blended with PBT to prepare PBT/PEGMA and PBT/Clay, respectively. The morphology was investigated by wide-angle X-ray diffraction (WAXD), scanning electron microscopy (SEM), and transmission electron microscopy (TEM). The clays were aggregated together and phase separation was observed in PBT/Clay. The clays were exfoliated in PBT/PEGMA/Clay. The equilibrium melting temperature was estimated by linear and nonlinear Hoffman-Weeks relation. The influence of the PEGMA and clay on the PBT crystallizable ability was also investigated by Avrami model and undercooling (difference between crystallization and equilibrium melting temperature). Hoffman-Lauritzen relation was used to estimate chain fold surface free energy. The exfoliated silicates cause a large number nucleus center to enhance the crystallization in PBT/PEGMA/Clay. The presence of PEGMA can react with the PBT and an increase in viscosity would reduce molecular mobility and crystallization in PBT/PEGMA. The aggregated clays have a confinement effect on the segmental motion of PBT and hinder the crystallization in PBT/Clay. © 2008 Wiley Periodicals, Inc. J Appl Polym Sci 110: 2195–2204, 2008

Key words: clay; crystallization; dispersions; nanocomposites

INTRODUCTION

Nanocomposites of organic/inorganic have been studied by many researchers because they often exhibit unexpected hybrid properties synergistically derived from the two components.[1–5] The enhancement of functional properties is achieved with the inclusion of only small amount of nanoscale inorganic materials.

Poly(butylenes terephthalate) (PBT) is an importance thermoplastic material for a large number of applications because of its good combination of properties, such as rigidity and solvent resistance. Some nanocomposites based on PBT have been reported.[6–8]

Polymer/clay nanocomposites have attracted most attention because the dispersion of nanoscale clay can improve the thermal stability,[9] mechanical strength,[10] molecular barrier,[11] and flame resistance[12] properties of polymers. The dispersion of nanoparticles is the most important subject in studying how to apply nanoparticles technology successfully to polymers.[13,14] To improve the lamellae exfoliation, or intercalation to increase the polymer adhesion to the mineral filler, several methods have been used to obtain polymer/clay nanocomposites, such as solution intercalation, melt intercalation, and, *in situ* interlayer intercalation.[15–19]

Some researchers tried to prepare polymer/clay nanocomposites by using a functional oligomer as a compatibilizer, such as maleic anhydride grafted polypropylene,[20] poly(ε-caprolactone),[21] and epoxypropyl methacrylate.[22] The compatibilizer should be an important factor for properties of nanocomposites because it will influence the dispersion of nanoscale particle and the crystallization. Most research have focused on the effects of compatibilizer on the dispersion,[15–22] but the question of how crystallization is affected by a compatibilizer is much less studied.

In our previous articles,[23,24] a commercially modified clay can be exfoliated by poly(ethylene-*co*-glycidyl methacrylate) (PEGMA) via an extruder, and the dispersion of silicates were also studied. In this article, PEGMA was used as a compatibilizer to disperse commercial modified montmorillonite clays in PBT. The dispersion of clays in matrix was observed by wide-angle X-ray diffraction (WAXD), scanning

Correspondence to: J.-W. Huang (jw.huang@msa.hinet.net).

electron microscopy (SEM), and transmission electron microscopy (TEM). The effects of dispersed silicates on the equilibrium melting temperature, crystallization rate, and chain fold surface free energy were examined by Avrami model, Hoffman-Weeks relation, and Hoffman-Lauritzen relation. The individual PEGMA and clay on those properties were also investigated.

EXPERIMENTAL

Materials

Commercial grade poly(butylene terephthalate) (PBT) was supplied by Chang Chun Group (Taipei, Taiwan) under trade name PBT1100-211M with a melt flow index (MFI) of 18–22 g/10 min. (508 K $\times$ 2.16 kgf, ASTM D1238). Commercial grade poly (ethylene-*co*-glycidyl methacrylate) (CG5004) was supplied by Sumitomo Chemical Co (Tokyo, Japan), which contains 81 wt % ethylene and 19 wt % glycidyl methacrylate. Commercial modified montmorillonite clay was purchased from Vulchem (Taipei, Taiwan, Trade Name: KH-γc) and more information was described in the earlier articles.[23,24] Both materials were used as received without purification.

Sample preparation

All materials were dried at 323 K in a vacuum oven for 6 h before compounding. PEGMA and 20 wt % clay were compounded with twin-screw extruder ($L/D = 32$, $D = 40$ mm, Continent machinery company, model CM- MTE 32) at 453 K and 300 rpm to make a master batch. The master batch was then mixed with 90 wt % PBT and re-compounded at 523 K and 100 rpm to prepare PBT/PEGMA/Clay nanocomposite, which contains 2 wt % clay, 8 wt % PEGMA, and 90 wt % PBT. Two blends of PBT/PEGMA and PBT/Clay were also prepared with 10 wt % PEGMA and 2 wt % clay, respectively, via a twin-screw extruder at 523 K and 100 rpm. On the basis of comparison, the neat PBT was also passed through the extruder at the same conditions.

Wide-angle X-ray diffraction

Wide-angle X-ray diffraction (WAXD) were carried out using a Philips XRG-3000 generator with Ni filtered CuKα radiation ($\lambda = 1.54$ Å) which operated at an applied voltage of 30 kV and a current of 30 mA. The patterns were recorded at a scanning rate of 1°/min over an angular range 1° to 10°.

Morphology

To characterize the morphology of the blends, the samples were fractured in liquid nitrogen and examined with scanning electron microscope (TOPCON ABT-150S). TEM observations are performed on a JEOL JEM 1200-EX TEM with an accelerating voltage of 80 kV.

Fourier transform infrared spectroscopy

Fourier transform infrared spectroscopy (FTIR) was carried out using a Spectrum RX1 FTIR apparatus. Thin films of the pure polymers and several blend systems were scanned with 50 scans per spectrum and a gain of 2.[13]

C CP/MAS NMR measurements

Solid-state ^{13}C MAS NMR measurements were carried out by using a BRUKER AVANCE 400. Magic angle spinning (MAS) was performed at 5 kHz spinning rate in the ^{13}C (at 75.4 MHz). The contact time in the ^{13}C CP (cross polarization) MAS NMR studies was 5 ms. All solid experiments were done at ambient temperature.

Isothermal crystallization

The crystallization behaviors of the PBT and PBT blends were investigated with a differential scanning calorimeter, Perkin–Elmer DSC-1. The differential scanning calorimeter was calibrated using indium with samples weights of 8–10 mg. All operations were carried out in a nitrogen atmosphere. Before data gathering, the samples were heated to 583 K and held in the molten state for 5 min to eliminate the influence of thermal history. The sample melts were then subsequently quenched at a rate of 100 K/min to reach the specific temperatures. When the isothermal crystallization had completed, the samples were heated to 583 K at a rate of 10 K/min to measure the melting temperatures.

RESULTS AND DISCUSSION

WAXD

Figure 1 shows the WAXD patterns for the commercial modified clay, neat PBT, PBT/PEGMA, PBT/Clay, and PBT/PEGMA/Clay. There is no obvious X-ray diffraction peak at the low 2θ range (1–10°) in neat PBT, PBT/PEGMA, and PBT/PEGMA/Clay. The modified clay exhibits a single peak at $2\theta = 7.27°$ (12.15 Å basal space) which is from (001) plane of the clay before compounding. As shown in Figure 1, PBT/Clay shows a peak $2\theta = 7.2°$ which is similar to that of modified Clay. It indicates that the melt compounding do not increase interlayer spacing of the clay. Compared with that of PBT/Clay, there is no peak for the PBT/PEGMA/Clay nanocomposite in the range of 1°–10°; indicating that the

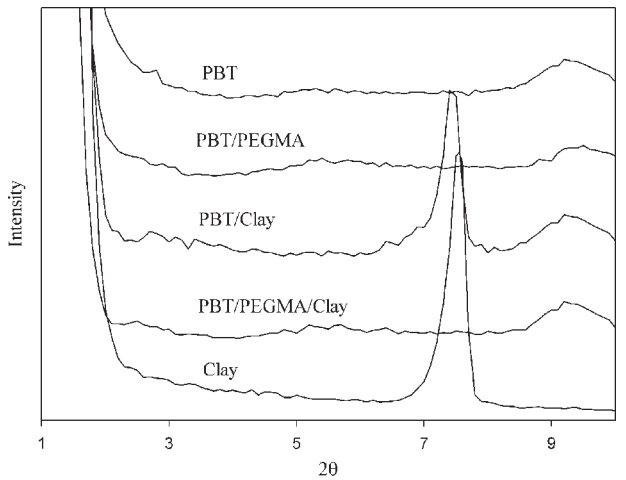

Figure 1 WAXD pattern of PBT, PBT/PEGMA, PBT/Clay, and PBT/PEGMA/Clay.

basal spacing (001) of the nanoclays in the PBT/PEGMA/Clay nanocomposite is larger than 80 nm. The commercial modified clay seems to be delaminated in PBT/PEGMA/Clay.

Morphology

The cryogenically fractured surfaces of blends of PBT/PEGMA, PBT/Clay, and PBT/PEGMA/Clay are shown in Figure 2(a–c). There is no obvious phase separation in PBT/PEGMA [Fig. 2(a)], it may be because of a reaction taking place between the PBT end groups and the epoxide ring at interface which is believed to be a ring opening reaction according to a nucleophilic substitution mechanism, as shown in Scheme 1.[25]

Figure 3(a) shows the spectra of pure PBT, PEGMA, and PBT/PEGMA. PEGMA clearly displays

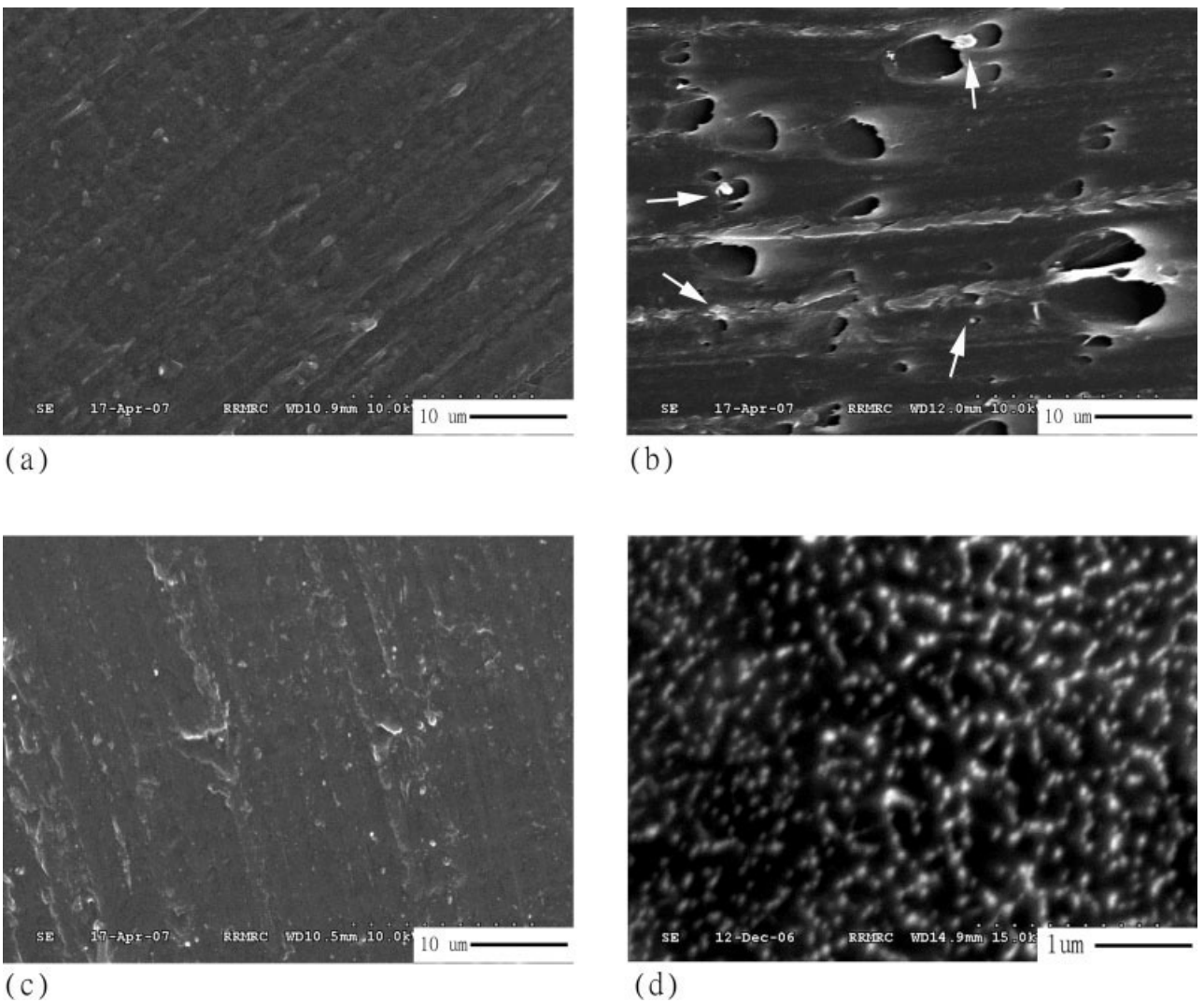

Figure 2 SEM micrograph of PBT blends. (a) PBT/PEGMA, (b) PBT/Clay (clay is indicated by an arrow), (c) PBT/PEGMA/Clay, (d) PBT/PEGMA/Clay (high magnification).

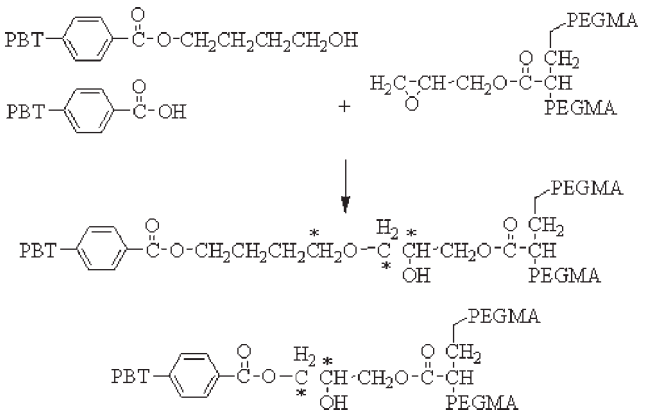

Scheme 1 Reaction of PBT and PEGMA.

the presence of epoxide FTIR bands positioned at 994, 912, and 843 cm^{-1}.[26] The three characteristic peaks of epoxy groups disappear in the IR spectra of PBT/PEGMA which can be attributed to the reaction between the PBT and PEGMA. The reaction at interface induces partial miscibility between PBT and PEGMA.

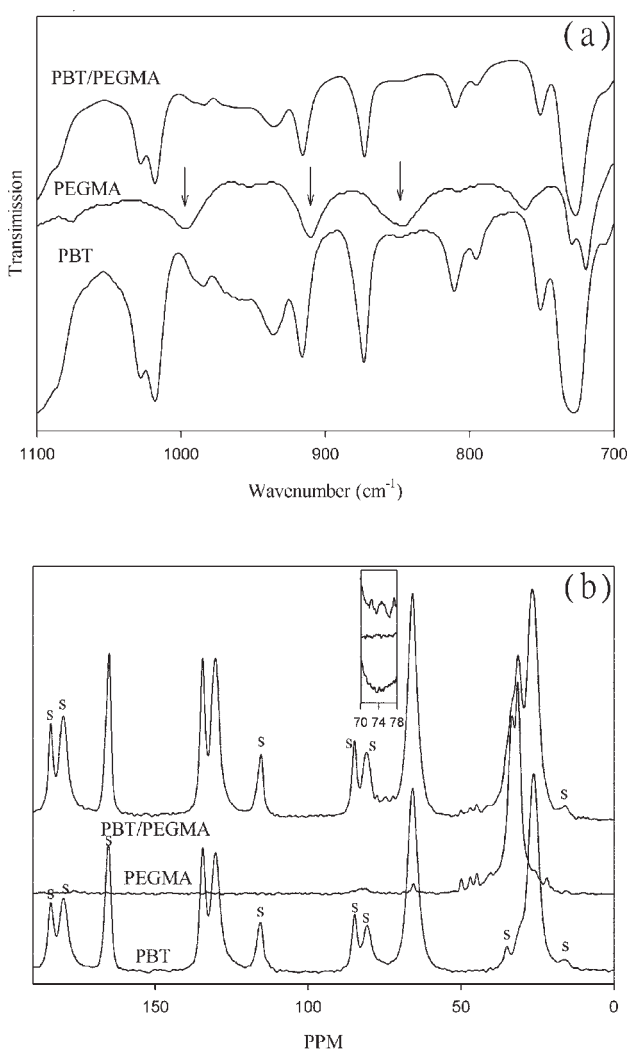

Figure 3 FTIR and ^{13}C CP/MAS NMR of neat PBT, PEGMA, and PBT/PEGMA blend. (a) FTIR, (b) ^{13}C CP/MAS NMR. The sideband patterns, mainly due to the carbonyl carbon, are indicated by "S."

Figure 3(b) shows the spectra of ^{13}C CP/MAS NMR. As compared with neat PBT and PEGMA, some small chemical shifts in PBT/PEGMA appear between 70 and 78 ppm. Those signals should be the chemical shifts of "C*" as a result of the reaction between the PBT and PEGMA[27] shown in Scheme 1.

Figure 2(b) exhibits obvious phase separation between clays and PBT in PBT/Clay blend. The silicate cannot be intercalated or exfoliated by PBT. Figure 2(c) reveals a homogeneous dispersion of silicate in matrix and no obvious phase separation is observed. When the PBT/PEGMA/Clay was observed at higher magnification [Fig. 2(d)], the silicate was dispersed like fibril in the matrix. In Figure 4, the TEM image of PBT/PEGMA/Clay exhibits a nanoscale dispersed morphology containing individual silicate, which is consistent with the previous observation of WAXD. The silicate was exfoliated in PBT/PEGMA/Clay.

Equilibrium melting temperature

The equilibrium melting temperature (T_m^o) of a polymer is defined as the melting temperature of an infinite stack of extended chain crystals, large in directions perpendicular to the chain axis and where the chain ends have established an equilibrium state of pairing. The equilibrium temperature is a true reflectance of a microstructure and the morphology of a blend, and it is a reference temperature and act as the driving force for crystallization.[28–30]

To estimate equilibrium melting temperature(T_m^o), the Hoffman-Weeks relation[31] has been extensively

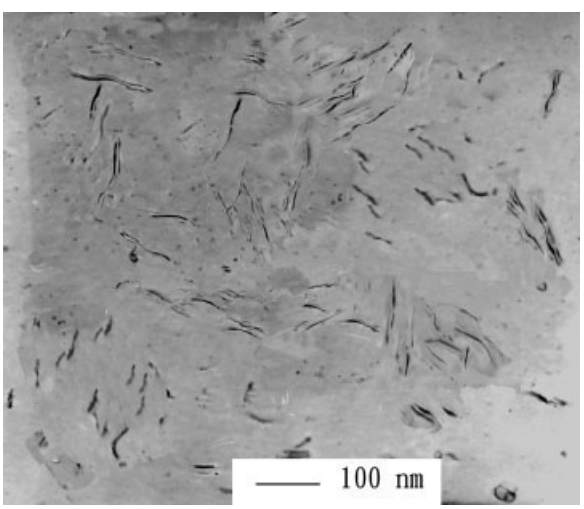

Figure 4 TEM micrograph of PBT/PEGMA/Clay nanocomposite.

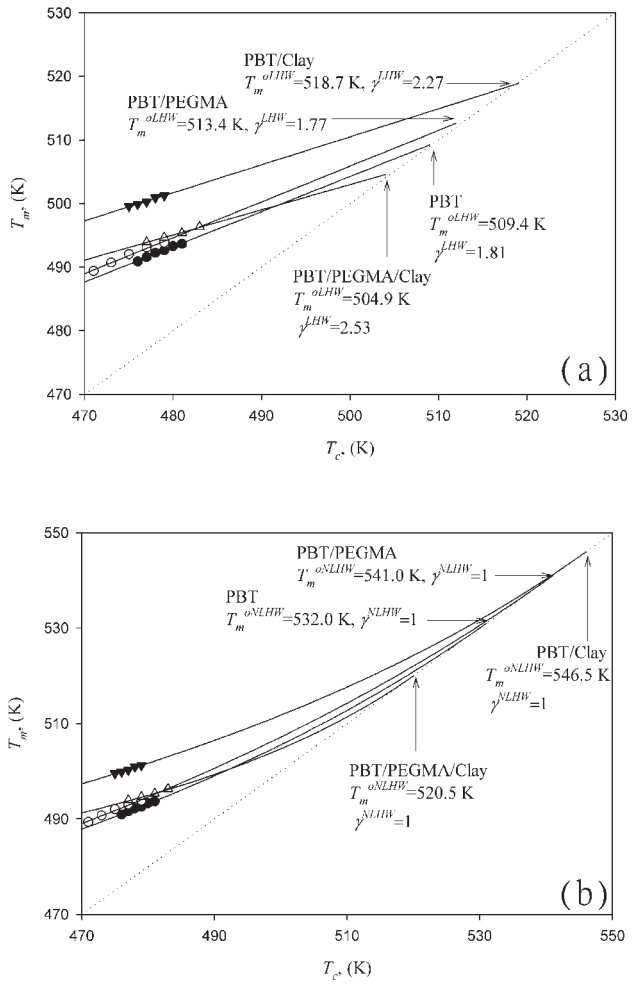

Figure 5 (a) T_m^{oLHW} obtained from linear HW plots. (b) T_m^{oNLHW} obtained from nonlinear HW.

accepted, which is determined by extrapolation of T_m versus T_c to $T_m = T_c$ (called linear HW; LHW)

$$T_m' = T_m^{oLHW}\left(1 - \frac{1}{\gamma^{LHW}}\right) + \frac{T_c}{\gamma^{LHW}} \quad (1)$$

The thickening coefficient $\gamma^{LHW} = l/l^*$, where l and l^* are the lamellar thickness at the time of melting and the thickness of the critical nucleus at T_c, respectively. The linear Hoffman-Weeks plots obtained by DSC are shown in Figure 5(a). From the linear H-W analysis, T_m^{oLHW} values are 509.4, 513.4, 518.7, and 504.9 K, and the γ^{LHW} values are 1.81, 1.77, 2.27, and 2.53 for PBT, PBT/PEGMA, PBT/Clay and PBT/PEGMA/Clay, respectively. The T_m^{oLHW} value of neat PBT is similar to that (509 K) reported by Runt et al.[32] The γ^{LHW} values greater than one are physically meaningless, as it would imply rapid and significant thickening of polymer lamellae at a very short time after their formation.

Alamo et al.[33] has explained the nonlinearity in the observed T_m and T_c. l^* should be dependent on the degree of undercooling ($\Delta T = T_m - T_c$) and $l^* = C_1/\Delta T + C_2$, where C_1 and C_2 are constant. But C_2 is always ignored in linear HW. Marand et al.[34] proposed the following equation (nonlinear H-W; NLHW) to improve the linear Hoffman-Weeks relation:

$$M = \gamma^{NLHW}\left(\frac{\sigma_e^l}{\sigma_{em}}\right)(X + a) \quad (2)$$

$$M = \frac{T_m^{oNLHW}}{T_m^{oNLHW} - T_m} \quad (2a)$$

$$X = \frac{T_m^{oNLHW}}{T_m^{oNLHW} - T_c} \quad (2b)$$

$$a = \frac{\Delta H_f C_2}{2\sigma_e^l} \quad (2c)$$

where T_m^{oNLHW} is the equilibrium melting temperature for nonlinear Hoffman-Weeks equation, γ^{NLHW} is the thickening coefficient, σ_e^l is the interfacial energy associated with the basal plane of the mature crystallite, σ_{em} is the fold surface free energy associated with a nucleus of critical size including the extra lateral surface energy due to fold protrusion and the mixing entropy associated with stems of different lengths and ΔH_f is the heat of fusion of crystal. σ_e^l is assumed to be equal to σ_{em} for most cases.[34] According to eq. (2), a constant γ^{NLHW} was estimated from the plot of M versus X for a specified T_m^{oNLHW}. The "true" equilibrium melting temperature (T_m^{oNLHW}) by this method was found when $\gamma^{NLHW} = 1$ (as shown in Fig. 6). The nonlinear H-W plot is also shown in Figure 5(b) and the T_m^{oNLHW} values are 532.0, 541.0, 546.5, and 520.5 K for PBT, PBT/PEGMA, PBT/Clay, and PBT/PEGMA/Clay, respectively. There is an apparent difference between the

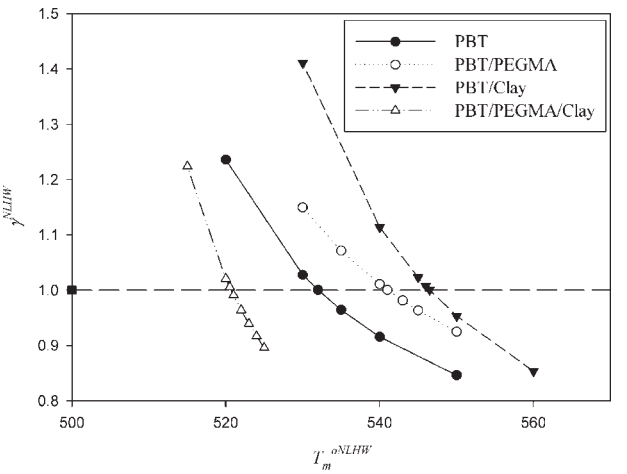

Figure 6 Calculated thickening coefficients at different specific equilibrium melting temperature.

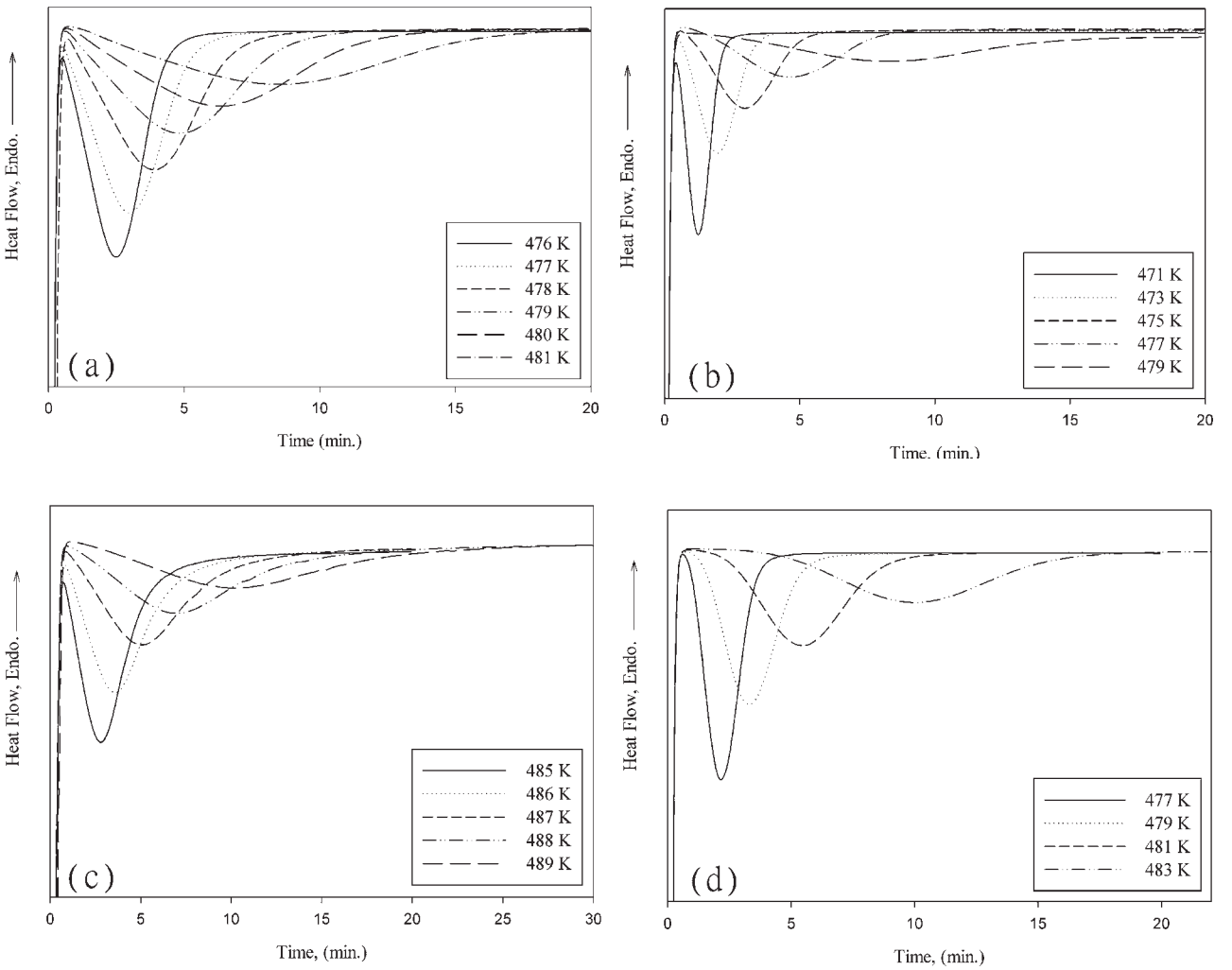

Figure 7 DSC isothermal measurement curves for PBT and PBT/Clay blends. (a) PBT, (b) PBT/PEGMA, (c) PBT/Clay, (d) PBT/PEGMA/Clay.

linear H-W and nonlinear H-W, the nonlinear H-W estimate being higher in all samples.

The equilibrium melting temperature (T_m^{oLHW} or T_m^{oNLHW}) of PBT/PEGMA and PBT/Clay blend are higher than that of neat PBT. A chemical reaction taking place between PBT and PEGMA in PBT/EGMA results in an increase of the blend viscosity, and molecular chains become harder to melt.[25] The addition of clay would hinder the molecular mobility and molecular chain becomes "stiffer." Clark and Hoffman[35] thought that a stiffer chain would result in a higher T_m^o and that the work of chain folding would also increase because the stiffer chain is harder to bend to make the fold. These results are also confirmed by following work on fold surface free energy. The exfoliated silicate would induce more nuclei to crystallize, but at the same time destroy the perfectness of crystal. The exfoliated silicate acts as a nucleating agent to cause a large number of crystals to grow in a limited space. Therefore, the large number of nucleus centers causes more crystalline defects and more imperfect crystals were formed and a lower T_m^{oLHW} or T_m^{oNLHW} is observed in PBT/PEGMA/Clay. Similar phenomenon was also observed in polystyrene/clay nanocomposites.[36]

Isothermal crystallization

The isothermal crystallization DSC curves for the neat PBT and the PBT blends are shown in Figure 7(a–d). A sample with higher crystallization temperature requires a longer time to complete crystallization. Crystallinity (X_t) was calculated as the ratio of the exothermic peak areas at time t and infinite time[37–39]:

$$X_t = \frac{\int_0^t \left(\frac{dH_c}{dt}\right) dt}{\int_0^\infty \left(\frac{dH_c}{dt}\right) dt} \quad (3)$$

where dH_c is the enthalpy of crystallization released during an infinitesimal time interval dt. Figure 8(a–d)

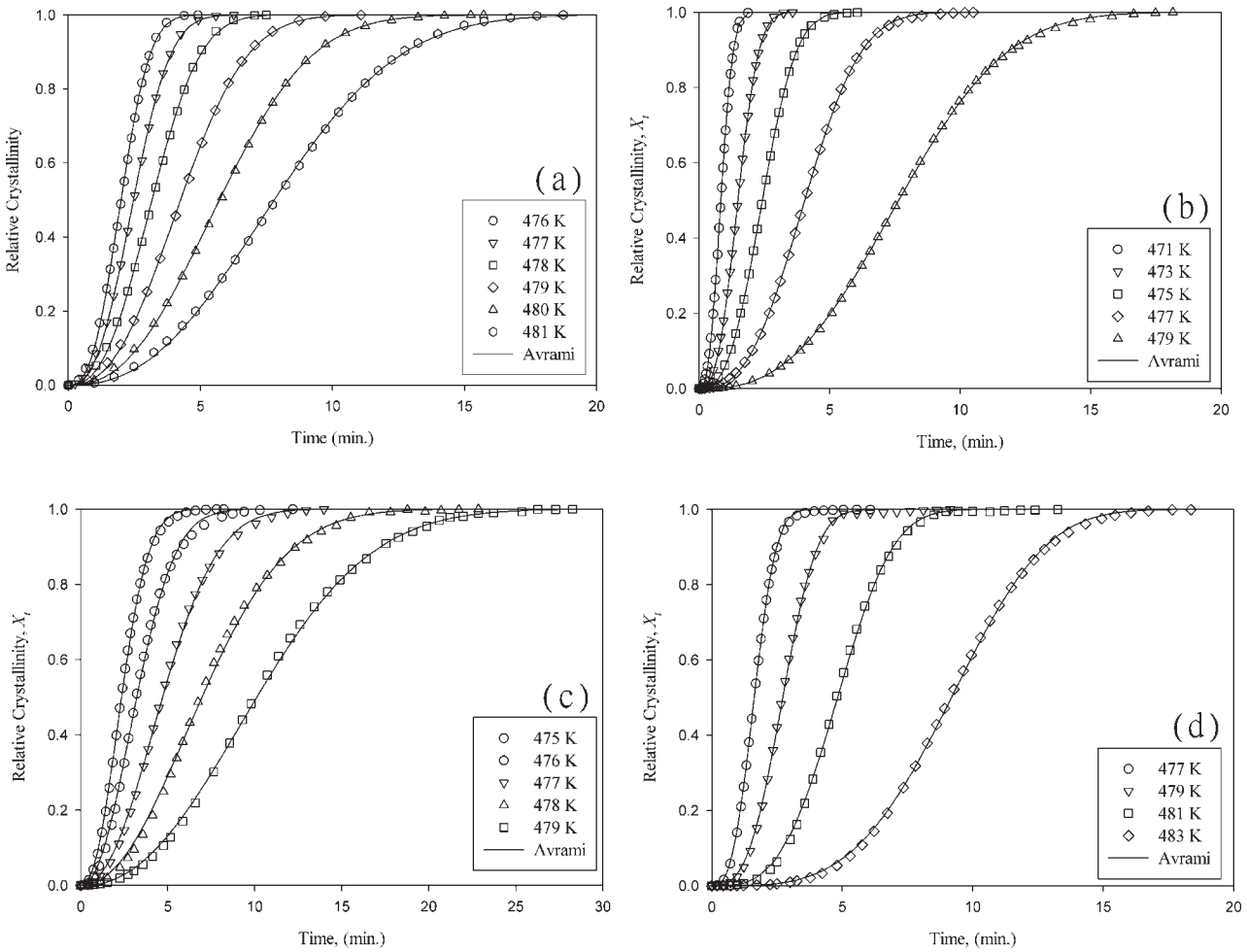

Figure 8 Relative crystallinity as a function of crystallization temperature. (a) PBT, (b) PBT/PEGMA, (c) PBT/Clay, (d) PBT/PEGMA/Clay.

shows the relative crystallinity of neat PBT and PBT blends. From these curves, the half-time of crystallization $t_{1/2}$, defined as the time required to reach half crystallinity ($X_t = 0.5$) can be computed. In general, $t_{1/2}$ or $1/t_{1/2}$ is taken as a measure of the overall rate of crystallization of a polymer as shown in Table I. It can be seen that $1/t_{1/2}$ of PBT decreases with the increasing T_c, which indicates that the total crystallization time is lengthened and that the crystallization rate decreases with increasing T_c. The $1/t_{1/2}$ value of each specimen will be compared under considering undercooling ($\Delta T = T_m^o - T_c$) in next section.

Avrami model

By assuming that the relative crystallinity increased with an increase in the crystallization time t, the Avrami equation can be used to analyze the isothermal crystallization process of polymers[37–39]:

$$X_t = 1 - \exp(-(K_a t)^{n_a}) \quad (4)$$

where X_t is the relative crystallinity, t is crystallization time, K_a is the Avrami crystallization rate constant and n_a is the Avrami exponent. X_t can be calculated as the ratio between the area of the exothermic peak at time t and the total measured area of crystallization. Values of K_a and n_a were found by fitting experimental data of X_t to eq. (4) and the results were shown in Table I. The regression coefficients listed in Table I show that the fitting between the data and model is very good. On the basis of the kinetic results summarized in Table I, to reconstruct the relative crystallinity as a function of time for each temperature (as shown in Fig. 8) also shows very good consistency between the data and Avrami model [eq. (4)] throughout the range.

Avrami exponent (n_a) represents a parameter revealing the nucleation mechanism and growth dimension. The n_a values for neat PBT in Table I are 2.42–2.65, which are close to those reported by Chou

TABLE I
Kinetic Parameters of PBT and PBT Blends

Sample	T_c (K)	K_a, min^{-1}	n_a	R^2	$t_{1/2}$, min	$1/t_{1/2}$, min^{-1}
PBT	476	0.4374	2.65	0.9997	2.01	0.50
	477	0.3521	2.58	0.9997	2.49	0.40
	478	0.2737	2.55	0.9996	3.20	0.31
	479	0.2031	2.47	0.9998	4.28	0.23
	480	0.1504	2.42	0.9998	5.75	0.17
	481	0.1104	2.43	0.9998	7.85	0.13
PBT/PEGMA	471	1.0450	2.61	0.9999	0.83	1.20
	473	0.5885	2.73	0.9999	1.49	0.67
	475	0.3614	2.73	0.9999	2.43	0.41
	477	0.2165	2.75	0.9999	4.05	0.25
	479	0.1143	2.71	0.9999	7.63	0.13
PBT/Clay	475	0.3919	2.22	0.9996	2.33	0.43
	476	0.2918	2.13	0.9989	3.17	0.32
	477	0.2290	2.19	0.9994	4.65	0.22
	478	0.1608	2.11	0.9986	6.84	0.15
	479	0.1241	2.26	0.9994	9.01	0.11
PBT/PEGMA/Clay	477	0.5396	2.82	0.9998	1.62	0.62
	479	0.3256	3.00	0.9994	2.70	0.37
	481	0.1856	3.28	0.9994	4.78	0.21
	483	0.0986	3.26	0.9998	9.93	0.10

et al.[40] The n_a values for PBT/PEGMA are 2.61–2.75. The values of both samples are between two and three, which are attributed to truncated spheres resulting from instantaneous nucleation with diffusion control.[41,42] The n_a values of PBT/Clay are 2.11–2.26 which are close to two and might correspond to two dimensional growth. For PBT/PEGMA/Clay, the values are 2.82–3.28 which are close to three, and it might correspond to an athermal nucleation and three-dimensional growth.

The crystallization rate K_a depends strongly on T_c. The isothermal rate constants, K_a, are also shown in Table I as a function of T_c for all samples. It can be seen that the values of K_a, crystallization rates, increases with decreasing T_c. To compare the crystallizable ability, the undercooling should be considered. The undercooling dependence of crystallization rate (K_a) could be obtained as shown in Figure 9. The K_a values increases with increasing ΔT. At a specific K_a value, the ΔT follows the order: PBT/Clay > PBT/PEGMA > PBT > PBT/PEGMA/Clay, which indicates the crystallizable ability is ranked: PBT/PEGMA/Clay > PBT > PBT/PEGMA > PBT/Clay. Figure 9 also shows the undercooling dependence of $1/t_{1/2}$, and similar results were obtained as K_a values. The crystallizability is controlled by nucleation and diffusion of molecular chains. The addition of PEGMA can react with PBT and lead to an increase of the blend viscosity, rendering the chains less mobile and lower the crystallizability of PBT/PEGMA. The clay in PBT can act as a nucleating agent to increase the crystallization rate, but at the same time hinder the molecular motion to retard the crystallization. The exfoliated silicate in PBT/PEGMA/Clay functions as nuclei and enhances the crystallization.

Lauritzen and Hoffman theory

The overall crystallization rate should be interpreted by the combination of nucleation and growth phenomena. Hoffman-Lauritzen[43] proposes the following equation:

$$\psi(T_c) = \psi_0 \exp\left[\frac{-U^*}{R(T_c - T_\infty)} - \frac{K_g}{T_c(\Delta T)f}\right] \qquad (5)$$

where $\psi(T_c)$ is crystallization rate parameter and ψ_0 is a preexponential term; $U^* = 1500$ cal/mol is the diffusional activation energy for the transport of

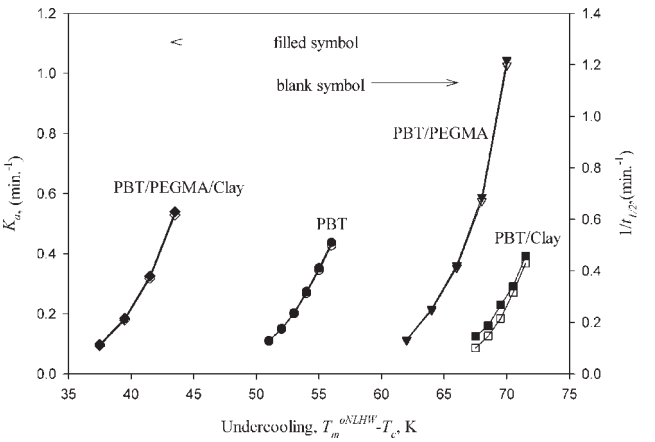

Figure 9 Relation of undercooling and rate constants evaluated from Avrami model (K_a) and $1/t_{1/2}$.

crystallizable segments at the liquid-solid interface; R is the gas constant; $T_\infty = T_g - 30K$ is the hypothetical temperature below which viscous flow ceases; T_g is glass transition temperature of PBT[44–47] and T_g = 248 K seems to be reasonable.[44,45] $\Delta T = T_m^o - T_c$; $f = 2T_c/(T_m^o + T_c)$ is a correction factor; K_g is the nucleation parameter which can be related to the product of lateral and folding surface free energy.

The crystallization rate parameter $\psi(T_c)$ could be considered proportional to $1/t_{1/2}$, eq. (5) can be rewritten as:

$$\frac{1}{t_{1/2}} = \psi_0 \exp\left[\frac{-U^*}{R(T_c - T_\infty)} - \frac{K_g}{T_c(\Delta T)f}\right] \quad (6a)$$

or

$$\ln\left(\frac{1}{t_{1/2}}\right) + \frac{U^*}{R(T_c - T_\infty)} = \ln \psi_o - \left(\frac{K_g}{T_c(\Delta T)f}\right) \quad (6b)$$

Figure 10 shows the plot of eq. (6b) for PBT and PBT blends by using $T_m^o = T_m^{oNLHW}$. The K_g could be obtained from the slope and intercept of Figure 10 and the results were listed in Table II. The K_g value of PBT is higher than those reported in literature[48,49] since the T_m^o estimated from nonlinear HW (T_m^{oNLHW}) is higher than linear HW (T_m^{oLHW}). When $T_m^o = T_m^{oLHW}$ was used, the K_g value (1.36×10^5) was close to that literature data (1.35×10^5)[40] in crystallization regime III of PBT.

The obtained K_g values can be used to determine the fold surface free energy (σ_e):[43]

$$K_g = \frac{jb\sigma\sigma_e T_m^o}{k\Delta h_f} \quad (7)$$

where b is the width of the chain, 5.17×10^{-10} m for PBT[48]; $\sigma = 8.8$ erg/cm^{-2} for PBT[48]; k is the Boltzman

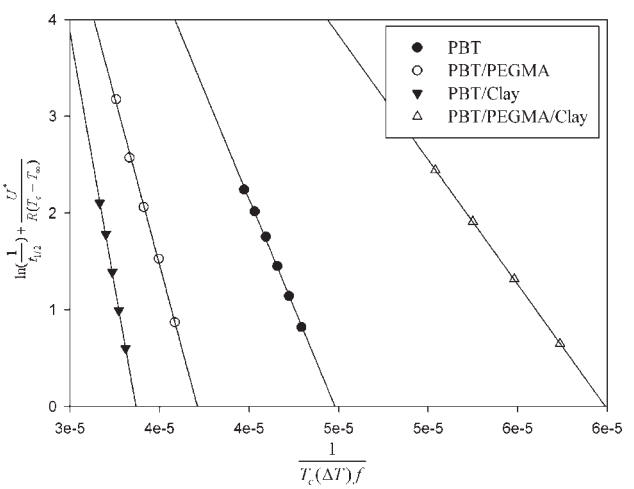

Figure 10 Lauritzen-Hofmann plots for isothermal crystallization of PBT and PBT blends.

TABLE II
Nucleation Rate Constant and Surface Free Energies for PBT and PBT Blends

Sample	$K_g \times 10^{-5}$ (K^2)	$\sigma\sigma_e \times 10^{-4}$ (J^2/m^4)	σ_e (erg/cm^2)
PBT	4.47	11.20	114.3
PBT/PEGMA	6.92	17.05	174.0
PBT/Clay	10.49	25.58	261.6
PBT/PEGMA/Clay	2.57	6.58	67.1

constant; and Δh_f is the the enthalpy of fusion, $\Delta h_f = 1.98 \times 10^8$ J/m^3[40,48]; j is a variable that depends on crystallization regime and is equal to 4 for regimes I and III, and 2 in regime II. Three different regimes can be developed during polymer crystallization, depending on the competition between the rate of secondary nuclei and the rate of lateral surface spreading.[39] There are two separate T_c ranges for PBT, ranging from 459 to 483 K (regime III), and from 485 to 491 K (regime II). There is a regime II-III transition at 484 K[45]; hence the experimental data in present work belongs regime III and $j = 4$. The fold surface free energy (σ_e) was estimated by eq. (7) and tabled in Table II. The σ_e value is influenced by nucleating effect and the mobility of polymer chains. The molecular mobility is reduced and a higher σ_e value is obtained with the addition of PEGMA because a chemical takes place between two components and the viscosity increases in PBT/PEGMA. A confinement effect of clay on the segmental motion of PBT hinders the crystallization and a higher σ_e value is observed in PBT/Clay. The clay is exfoliated in PBT/PEGMA/Clay and causes a large number of nucleuses centers. The nucleation effect becomes more evident in PBT/PEGMA/Clay, which is probably the main reason for the reduced σ_e value.

CONCLUSIONS

PBT/clay nanocomposite has been prepared successfully by blending PBT and commercially available montmorillonite clays via a twin-screw extruder by using PEGMA as a compatibilizer. Exfoliated silicate is well dispersed in PBT/PEGMA/Clay from the investigation of WAXD and TEM. The clays aggregate together and exhibit phase separation in PBT/Clay without PEGMA. Crystallizability of the composite is estimated by the Avrami model under same degree of undercooling and follows the order: PBT/PEGMA/Clay > PBT > PBT/PEGMA > PBT/Clay. The presence of exfoliated silicate enhanced the crystallization, but the PEGMA and aggregated clays retarded the crystallization consistent with the fold surface free energy (σ_e) estimated from Hoffman-Lauritzen relation. A chemical reaction taking place between PBT and PEGMA increased the

viscosity and render the chains less mobile; the polar group of PEGMA also gives rise to a higher σ_e. The aggregated clays in PBT/Clay have a confinement effect on the segmental motion of PBT and thus hinder the crystallization and a higher σ_e value is observed. The clay is exfoliated in PBT/PEGMA/Clay and causes a large number of nuclei centers to enhance the crystallization, and the σ_e value is reduced.

References

1. Yano, K.; Usuki, A.; Okada, A.; Kurauchi, T.; Kamigaito, O. J Polym Sci Part A: Polym Chem 1993, 31, 2493.
2. Giannelis, E. P. Adv Mater 1996, 8, 29.
3. Chang, J. H.; Seo, B. S.; Hwang, D. H. Polymer 2002, 43, 2969.
4. Yano, K.; Usuki, A.; Okada, A. J Polym Sci Part A: Polym Chem 1997, 35, 2289.
5. Yang, Y.; Zhu, Z.; Yin, J.; Wang, X.; Qi, Z. Polymer 1999, 40, 4407.
6. Li, X. C.; Kang, T.; Cho, W. J.; Lee, J. K.; Ha, C. S. Macromol Rapid Commun 2001, 22, 1306.
7. Tripathy, A. R.; Burgaz, E.; Kukureka, S. N.; Mac-Knight, W. J. Macromolecules 2003, 36, 8593.
8. Broza, G.; Kwiatkowska, M.; Roslaniec, Z.; Schulte, K. Polymer 2005, 46, 5860.
9. Lan, T.; Kaviratna, P. D.; Pinnavaia, T. J Chem Mater 1994, 6, 573.
10. Tyan, H. L.; Liu, Y. C.; Wei, K. H. Chem Mater 1999, 11 1942.
11. Wang, Z.; Pinnavaia, T. J. Chem Mater 1998, 10, 3769.
12. Gilman, J. W.; Jackson, C. L.; Morgan, A. B.; Hayyis, R. J.; Manias, E.; Giannelis, E. P.; Wuthenow, M.; Hilton, D.; Philips, S. H. Chem Mater 2000, 12, 1866.
13. Kawasumi, M.; Hasegawa, N.; Kato, M.; Usuki, A.; Okada, A. Macromolecules 1997, 30, 6333.
14. Kaempfer, D.; Thomann, R.; Mohlhaupt, R. Polymer 2002, 43, 2909.
15. Chang, J. H.; Kim, S. J.; Joo, Y. L.; Im, S. Polymer 2004, 45, 919.
16. Chang, J. H.; Park, K. M. Polym Eng Sci 2001, 41, 2226.
17. Vaia, R. A.; Ishii, H.; Giannelis, E. P. Adv Mater 1996, 8, 29.
18. Vaia, R. A.; Jandt, K. D.; Kramer, E. J.; Giannelis, E. P. Macromolecules 1995, 28, 8080.
19. Fukushima, Y.; Okada, A.; Kawasumi, M.; Kurauchi, T.; Kamigaito, O. Clay Miner 1988, 23, 27.
20. García-López, D.; Picazo, O.; Merino, J. C.; Pastor, J. M. Euro Polym J 2003, 39, 945.
21. Zheng, X.; Wilkie, C. A. Polym Degrad Stab 2003, 82, 441.
22. Liu, X.; Wu, Q. Polymer 2001, 42, 10013.
23. Huang, J. W.; Kang, C. C.; Chen, T. H. J Appl Polym Sci 2005, 97, 1051.
24. Huang, J. W.; Hung, H. C.; Tseng, K. S.; Kang, C. C. J Appl Polym Sci 2006, 100, 1335.
25. Loyens, W.; Groeninckx, G. Macromol Chem Phys 2002, 203, 1702.
26. Tsai, C. H.; Chang, F. C. J Appl Polym Sci 1996, 61, 321.
27. Wilhelm, M.; Neidhöfer, M.; Spiegel, S.; Spiess, H. W. Macromol Chem Phys 1999, 200, 2205.
28. Hoffman, J. D.; Davis, G. T.; Lauritzen, J. I. In Treatise on Solid State Chemistry; Hannay, N. B., Ed.; Plenum: New York, 1976; Vol. 3, Chapter 7.
29. Hoffman, J. D.; Miller, R. L. Polymer 1997, 38, 3151.
30. Xu, J.; Srinivas, S.; Marand, H.; Agarwal, P. Macromolecules 1998, 31, 8230.
31. Hoffman, J. D.; Weeks, J. J. J Res Natl Bur Stand 1962, 66A, 13.
32. Runt, J.; Milley, D. M.; Zhang, X.; Gallagher, K. P.; McFeaters, K.; Fishburn, J. Macromolecules 1992, 25 1929.
33. Alamo, R. G.; Viers, B. D.; Mandelkern, L. Macromolecules 1995, 28, 3205.
34. Marand, H.; Xu, J.; Srinivas, S. Macromolecules 1998, 31, 8219.
35. Clark, E. J.; Hoffman, J. D. Macromolecules 1984, 17, 878.
36. Wu, T. M.; Hsu, S. F.; Chien, C. F.; Wu, J. Y. Polym Eng Sci 2004, 44, 2288.
37. Avrami, M. J Chem Phys 1939, 7, 1103.
38. Avrami, M. J Chem Phys 1939, 8, 212.
39. Avrami, M. J Chem Phys 1939, 9, 177.
40. Chou, R. M.; Chang, C. C.; Yu, T. L.; Tseng, Y. H.; Wu, M. J Polym Int 2001, 50, 213.
41. Zhang, G.; Yan, D. J Appl Polym Sci 2003, 88, 2181.
42. Wunderlich, B. Macromolecular Physics; Academic Press: New York, 1976; Vol. 2.
43. Hoffman, J. D.; Frolen, L. J.; Ross, G. S.; Lauritzen, J. I. J Res NBS A 1975, 79, 671.
44. Cheng, S. Z. D.; Pan, R.; Wunderlich, B. Makromol Chem s 1988, 18, 2443.
45. Dilorenzo, M. L.; Righetti, M. C. Polym Eng Sci 2003, 43, 1889.
46. Boyer, R. F. Rubber Chem Technol 1963, 36, 1303.
47. Jackson, W. J.; Gray, T. F.; Caldwell, J. R. J Appl Polym Sci 1970, 14, 685.
48. Chen, X.; Xu, J.; Lu, H.; Yang, Y. J Polym Sci Part B: Polym Phys 2006, 44, 2112.
49. Righetti, M. C.; Munari, A. Macromol Chem Phys 1997, 198, 363.